

## **Dislocation junctions and jogs in a free-standing FCC thin film**

Seok-Woo Lee<sup>1,\*</sup>, Sylvie Aubry<sup>2</sup>, William D. Nix<sup>1</sup>, Wei Cai<sup>2</sup>

<sup>1</sup>*Department of Materials Science and Engineering, Stanford University, Stanford CA 94305-4034, United States*

<sup>2</sup>*Department of Mechanical Engineering, Stanford University, Stanford CA 94305-4040, United States*

### **Abstract**

Dislocation junctions and jogs in a free-standing FCC thin film have been studied using 3-dimensional dislocation dynamics simulations. Due to the unconstrained motion of surface nodes and dislocation annihilation at the free surface, junctions and jogs are unstable except for some uncommon conditions. If the film thickness is thin enough for a significant portion of dislocation network to be terminated at the free surface, junctions and jogs can exist for only a finite time during deformation. Thus, the creation of junction/jog-related dislocation sources and their performance are more limited as the film thickness decreases. This effect could lead to insufficient dislocation multiplication to balance dislocation annihilation at the free surface.

**Keywords:** dislocation, junction, jog, dislocation dynamics, thin film

**PACS code:** 62.20.F- Deformation and plasticity

## 1. Introduction

Thin film-based techniques have been used to produce device structures in emerging technologies, and the reliability of those devices is directly related to mechanical properties of their thin components [1]. These devices contain various metallic components, whose mechanical properties are governed primarily by dislocation mechanisms. Metallic thin films are commonly deposited onto substrates, in which case the mechanical properties of the film, especially the dislocation behavior within the film, are affected by constraining effects of the substrate and/or a passivation film. These constraining effects have been extensively investigated. However, the current technology calls for building more complex 3D structures, such as Micro-Electro Mechanical Systems (MEMS), so understanding the intrinsic mechanical properties associated with dislocation mechanisms in a free-standing thin film is also important for designing reliable mechanical devices at the small scale [2].

Dislocation junctions and jogs have been hypothesized as the primary dislocation structures needed to produce a dislocation source. These structures play an important role in forming the dislocation network and ultimately affect the global mechanical properties of a metal [3]. In a free-standing thin film, a large fraction of the dislocations is close to or intersect the two free surfaces. Due to the significant interaction between dislocations and free surfaces, the configuration of junctions and jogs would be expected to evolve differently, and would also result in a different mechanical response from those in a bulk metal. Therefore, an investigation of dislocation junctions and jogs associated with the free surface is needed to understand the intrinsic mechanical properties of a free-standing thin film.

In order to understand the micro-mechanics of dislocations, dislocation dynamics (DD) simulations have been developed actively [4-6]. The DD simulations allow us to follow the

evolution of dislocation structures in a reasonable spatial and temporal scale, compared to atomistic simulations and have been useful in finding new strengthening mechanisms in bulk metals [7, 8]. Furthermore, DD simulations have been used to interpret dislocation mechanisms at the small scale by incorporating image stress calculations [9-12]. Dislocation behaviors in a thin film have also been studied using both 2D and 3D simulations for various cases [13-17].

Recently, we implemented the Parallel Dislocation Simulator (ParaDiS) code [6], which was originally developed at the Lawrence Livermore National Laboratory (LLNL), on an efficient image stress calculation for the thin film geometry; we used the code to study an isolated single dislocation on one slip plane [9]. In this paper, we study dislocation junctions and glide-jogged dislocations in a free-standing FCC thin film. Their unique behaviors associated with the free surface will be examined. Then, the relation between the results and dislocation multiplication will also be discussed briefly.

## **2. Method**

The material parameters of FCC gold were used. The ParaDiS code uses isotropic elasticity, so the shear modulus was taken to be 27 GPa, and the Poisson's ratio is 0.44. The free surface of the film has the [001] orientation and the boundaries along [100] and [010] need to be periodic for the image stress calculation. The film thicknesses are 1  $\mu\text{m}$  for most calculations, and 0.5  $\mu\text{m}$  thickness is also used for one set of jog calculations to see the thickness dependence of jog mechanisms. The thin film in the computational cell has the aspect ratio of 10:1 (width/length : thickness). The ParaDiS code requires the dislocation core radius,  $a$ , and we assume  $a$  equals the magnitude of the Burgers vector of the perfect dislocation [18]. The FCC linear mobility law includes both a glide constraint and a line constraint. The glide constraint allows a dislocation to move only on its slip

plane to mimic the effect of the extended core structure of dislocations in FCC crystals, and the line constraint makes a Lomer-Cottrell (LC) junction immobile in the direction perpendicular to the line to take its non-planar core structure into account [3].

To investigate the behavior of dislocation junctions in a thin film, we studied two geometries. In the first case, the line of intersection of the two slip planes, the line along which a LC junction would form, is parallel to the plane of the film (figure 1(a)) and in the second case the line of intersection is inclined relative to the plane of the film (figure 1(b)). For the relaxation studies, the simulations begin with two straight dislocations which intersect at the mid-plane of the film. We also selected an intermediate junction structure during the relaxation, and then applied an in-plane uniform stress along the [100] direction to investigate the unzipping behavior of the junction configurations. In addition, in two simulations we intentionally make two mobile arms cross-slip to introduce a strong anchoring point for the gliding dislocation arms (figure 1(c)). The stability and source operation of these junctions were studied under a tensile stress of 300 MPa along the [010] direction.

We also studied the behavior of glide-jogged dislocations in free-standing thin films with two different thicknesses, 0.5 and 1  $\mu\text{m}$  (figure 2). The jog segment is located at the center of the film and is parallel to the free surface initially. For a given film thickness, the initial lengths of the dislocation arms are always the same, but jogs of different heights are considered. Because the jog is glissile, it can move and be annihilated at the free surface. This configuration is intentionally chosen to see the effects of the jog height and the possibility of source operation until the jog is annihilated. We applied stresses in the range from 10 to 800 MPa along [100] direction and also varied the jog height from  $5b$  to  $47b$ , where  $b$  is the magnitude of Burgers vector of the perfect dislocation. Finally, a mechanism map for 1  $\mu\text{m}$  was obtained with respect to the jog height and the applied stress.

### 3. Simulation Results

#### 3.1. Dislocation junctions in an FCC free-standing thin film

##### 3.1.1 Junction parallel to the plane of the film

The initial condition consists of two straight dislocations shown in figure 1(a). Dislocation (1) has the Burgers vector BC and glides on the ABC plane, while dislocation (2) has the Burgers vector CD and glides on the ACD plane. In order to create a dislocation junction, we intentionally inserted the dislocations with small angles  $\alpha$  and  $\beta$  (both are  $\pi/9$ ) relative to the line of intersection of the slip planes [19]. For this particular initial structure, the dislocation junction can never meet the free surface because the line direction of the junction is parallel to the plane of the film. The dislocations were first allowed to relax from the initial configuration under no applied stress.

During the relaxation, the two dislocations form a binary junction along the line of intersection of the slip planes (figure 3(b)). Then, the junction length begins to decrease, due to the line tension effect of the junction (figure 3(c)). In the case of a bulk metal, it is usually assumed that the four end nodes of dislocation arms are fixed by the rigid dislocation network [19], and the macroscopic strength is related to the breaking stress of this rigidly bound junction structure. In this study, however, because the four arms of the junction are terminated at the free surfaces, the motion of the surface node on the glide plane is not constrained. Thus, the junction can readily shrink. Finally, the junction is unzipped into the two separate dislocations that are now repulsive to each other (figure 3(d)), because they have rotated to a different orientation from the initial condition. Therefore, this junction is not stable in a free-standing thin film during relaxation (under zero stress).

We also studied the effect of an applied stress on the dislocation junction. Starting from a partly relaxed structure (figure 3(b)), uni-axial tensile stress was applied along the [100] direction. If the applied stress is low, the junction unzips as before. However, if the applied stress is high enough, the junction is unzipped by the bowing of dislocations arms, which is commonly observed in a bulk metal. We were unable to find any applied stress for which this junction can be stabilized in the thin film.

### 3.1.2. *Junction inclined relative to the plane of the film*

The initial configuration of two straight dislocations is shown in figure 1(b); dislocation (1) has the Burgers vector CA and glides on the ABC plane, while dislocation (2) has the Burgers vector BD and glides on the BCD plane. Here, the angles  $\alpha$  and  $\beta$  are again  $\pi/9$  (radian). This configuration produces a dislocation junction along the BC direction, which is inclined relative to the plane of the film (figure 4(b)). Because the four surface nodes are connected to the free surfaces, they can move freely. During relaxation, both dislocations completely zip into a junction line, threading through the film (figure 4(c)). If we assume the LC junction is immobile, then there is no mobile dislocation left in the film.

In order to study the effect of applied stress, uni-axial stresses along the [100] direction are applied to the intermediate configuration of figure 4(b). Under a low stress, the two dislocations zip into one junction in the same manner as in the relaxation case. However, if the stress level increases, the junction begins to be completely dissociated above a certain critical stress such as the common process. These results imply that the junction is either fully zipped or are completely unzipped according to the stress level. Therefore, this junction cannot maintain a structure with a junction connected to ordinary glissile dislocation arms such as in the bulk.

### 3.1.3. *Junction and cross-slip of dislocation arms: source operation*

To create a structure that is suitable for dislocation multiplication, we take the case of a junction parallel to the plane of the film, and let some of the mobile arms cross-slip onto other glide planes. Figure 1(c) shows the cross-slipped configurations we have considered. Here, dislocation (2) with Burgers vector  $CD$  cross-slips from the  $ACD$  plane to the  $CDI$  plane, or, equivalently, to the  $EFG$  plane. In this case, a stress is applied in the  $[010]$  direction, thus producing glide-forces on dislocation (2) but not (1). When only one lower arm is cross-slipped (cross-slip (L) in figure 1(c)), the unzipping process is still unavoidable. At the low stresses, the junction still shrinks because two mobile arms in the upper part of the configuration can move toward the cross-slipped arm. At high stresses, the common unzipping process occurs by the bowing motion of dislocation arm (2) in the upper part of the structure (figure 5). For a while, the cross-slipped arm can serve as the dislocation source for two reasons. First, the end node (E) of the junction acts as a strong pinning point, and the cross-slipped arm serves as a stable dislocation source (figure 5(b)). This end node (E) is the intersection point of three different slip planes. It cannot move without cross-slip or climb of a connected dislocation segment among three dislocations each having a different glide plane. Second, after the junction is completely unzipped, dislocation (2) has two arms on different slip plane, and becomes a dynamic dislocation source until the mobile cusp is annihilated at the free surface (figure 5(c) and (d)).

Depending on the position of the un-cross-slipped segment (dislocation (1) in figure (2)), the interaction with the cross-slipped arms can produce glissile dislocations, which can act as single arm dislocation sources. This configuration was also studied in DD simulations of micropillars [20,21]. Furthermore, in the unusual case where both arms of dislocation (2) are cross-slipped

(cross-slip (L) and (U) in figure 1(c)), the shrinkage does not occur because the glide constraint makes both end nodes immobile. Dislocations (1) and (2) react to form single dislocation arms at both ends of the junction, which have the Burgers vector  $BD$  and can glide on the CDI plane or, equivalently, the EFG plane. The end result is a jogged dislocation with Burgers vector  $BD$  having two single arm sources gliding on the CDI or EFG planes. Then, the two single arm sources would operate stably and continuously generate dislocations if the end nodes of the Lomer-Cottrell jog were assumed to be sessile. However, recent molecular dynamics simulations show that the Lomer-Cottrell jog can be mobile due to its constricted node [22].

### 3.2. Dislocation with glissile jog

The initial configuration of a jogged dislocation is described in figure 2. The two dislocation arms connecting the jog and the free surfaces have the Burgers vector  $CB$  and glide on the ABC plane. The jog has the same Burgers vector and is free to glide on the BCD plane. For a given film thickness and jog height, the dislocation structure evolves in the three different ways depending on the applied stress.

If the applied stress level is low, the dislocations arms cannot bow out and the jog rotates slightly on its slip plane. Then, one dislocation arm grows longer at the expense of the other arm, and the jog moves toward the free surface. Eventually the jog escapes from the film. Finally, only one threading dislocation remains. If the applied stress level is intermediate, the dislocation arms begin to bow out. The jog serves as an anchoring point for the two long mobile dislocation arms. Then, the two dislocation arms then will finally form a dipole, and later detaches from the gliding threading dislocation (figure 6(b)). The jog is glissile, so it moves toward the free surface in order to shorten the total length of the dipole. Finally, the dipole structure is annihilated at one of the free



surfaces, and only one threading dislocation remains without any jog on it. (The threading dislocation is not shown because it travelled out of the range of figure 6(b)). If the applied stress level is high enough to drive two dislocations arms of the dipole to pass each other, the dislocation structure can act as a dislocation source (figure 7). However, during the operation of the source, the jog moves around on its slip plane. After a finite time, the source structure is eventually destroyed when the jog collides with one of the free surfaces.

## **4. Discussion**

### *4.1. Dislocation junctions in an FCC free-standing thin film*

The simulation results for dislocation junctions that are parallel to the plane of the film showed that the junction is unstable under relaxation and under any applied stress state. In order to maintain the junction structure in figure 3(b), the two dislocation arms connected to the top surface need to experience a force in the opposite directions compared to the other two arms connected to the bottom surface. However, two mobile dislocation arms with the same character experience the same Peach-Koehler force under a uniform stress. Thus, it is impossible to lengthen the junction in a thin film under a uniform stress state, and the junction structure is eventually unzipped into the two threading dislocations, regardless of the stress level. The dislocation junction that is inclined relative to the free surface can also be analyzed in an analogous way. Therefore, when the junction structure is connected to the free surface, it is impossible to stabilize the dislocation junction structure. Instead, it could exist only for a finite period of time.

In order to stabilize the junction, the dislocation arms need to be cross-slipped. Then, the end node of junction can act as an anchoring point of dislocation source. In fact, the interaction with a third dislocation could produce a strong pinning point, but these two processes result in a final state similar with the cross-slip process [21]. A strain gradient, such as by bending or torsion, could also stabilize the junction structure because the stress state is inhomogeneous. We found that a bending moment can stabilize the junction structure. For the configuration in figure 3(b), if we apply the bending moment about  $[1 \bar{1} 0]$  direction larger than  $4.65 \mu\text{N}$  (per unit length along the edge), which corresponds to a maximum critical resolved shear stress of 11.4 MPa on ABC and ACD slip planes in figure 1, the junction length gets longer. Two dislocation arms connected to the top surface move in the opposite direction with those connected to the bottom surface. Thus, junction structures can be stabilized under an applied strain gradient.

For the cross-slip of the one arm (cross-slip (1) in figure 1(c)), the dislocation source is operative for a finite period of time (figure 5), and for the cross-slip of two arms (cross-slip (1) and (2) in figure 1(c)), the dislocation junction becomes an immortal source if we assume the LC segment moves only along its line direction. The latter case is probably rare because it is not likely that both arms would cross-slip at the same time. Since any junctions would exist for only a finite period time, the chance for cross-slip of dislocation arms or interaction with other dislocations would be even more limited. Hence, the probability of creating a permanent dislocation source in a free-standing thin film from junctions seems low. However, our simulations show that dislocation multiplication does occur for a limited period time, similar to that reported in [20].

#### 4.2. Dislocation jogs in a thin film

Our simulation show that the glide-jogged dislocation can evolve in three different ways with respect to the applied stress and the film thickness. From these results, mechanism map may be constructed for the 1  $\mu\text{m}$  thickness film, as shown in figures 8. This map shows that for a given jog height, the jog annihilates at low stresses, dipoles are formed at intermediate stresses and double arm sources operate at the highest stresses. The dipole formation involves the bowing motion of two dislocation arms, requiring a stress determined by the length of the dislocation arms, as in a Frank-Read source. Thus, the boundary (B1) between the region of ‘jog escape’ and ‘dipole formation’ is determined by the film thickness. However, the boundary (B2) between ‘dipole formation’ and ‘double arm source’ is determined by the jog height. The critical passing stress of two dislocation arms is inversely proportional to the jog height.

The stress level of B1 can be estimated by the operation stress of the Frank-Read source,

$$\sigma = \frac{\mu b}{l} \frac{1}{M}, \quad (1)$$

where  $\mu$  is the shear modulus (27 GPa),  $b$  is the magnitude of Burgers vector of the perfect dislocation ( $2.885 \times 10^{-10}$  m),  $l$  is the twice of the length of dislocation arm (or approximately the film thickness), and  $M$  is the Schmid factor (0.408). The estimated stress level is 19 and 38 MPa for film thicknesses 1 and 0.5  $\mu\text{m}$ , respectively. This estimate agrees well with the simulation result for a 1  $\mu\text{m}$  thick film, but shows some deviation from the simulation result for a 0.5  $\mu\text{m}$  thick film (75 MPa). As the film thickness decreases, the stress for bowing of the dislocation arms is more strongly affected by the image stresses, and may cause the deviation from equation (1). The axial stress level for B2 can be estimated by the critical passing stress of the two straight dislocations by

$$\sigma = \frac{\mu b}{8\pi(1-\nu)h} \frac{1}{M} = \frac{1.3565}{h \text{ (in m)}} \text{ (Pa)}, \quad (2)$$

where  $\nu$  is the Poisson's ratio, and  $h$  is the jog height. The location of B2 boundary does not change for both film thicknesses 1 and 0.5  $\mu\text{m}$ , indicating that the boundary B1 is independent of the film thickness from 0.5 to 1  $\mu\text{m}$ . Equation (2) agrees well with the simulation results for both 0.5 to 1  $\mu\text{m}$  thick films.

A glissile-jogged dislocation can act as the dynamical dislocation source when the applied stress level is above the boundary B2. Tensile deformation experiments on a Au thin film on a polyimide substrate showed that the axial flow stress at 0.5% strain is  $\sim 70$  MPa for 1  $\mu\text{m}$  thick films and  $\sim 100$  MPa for 0.5  $\mu\text{m}$  thick films [23]. For the given stress levels, the jog height corresponds to  $\sim 18$  nm ( $60b$ ) and  $\sim 14$  nm ( $46b$ ) for the source operation, respectively. At the experimental stress level, the jog height needs to exceed  $\sim 18$  nm ( $60b$ ) for source operation. It is unlikely to form such large jogs from the coalescence of unit jog produced by dislocation cutting each other. Hence, dislocation annihilation might be an important process for producing super jogs that are large enough to create dislocation sources.

#### *4.3. Dislocation multiplication in a free-standing thin film and the pinning points for stable dislocation sources*

The rapid annihilation rate of dislocations at the free surfaces may prevent an increase of dislocation density in a thin film. Since plastic deformation requires mobile dislocations, whether stable dislocation sources can exist in a thin film is an important question. Our simulation results show that junctions are not stable under a uniform stress state. Furthermore, a glide-jogged dislocation can only create a finite number of dislocations, and only if its height is sufficiently large or the applied stress is sufficiently high. These constraints become more pronounced in thinner

films. Thus, this effect could lead to conditions wherein dislocation multiplication cannot compensate dislocation annihilation at the free surfaces.

If the film is thick relative to the dislocation spacing, the junction structure could be connected to a dislocation network, instead of the free surface. This could make the junction sometime more stable, and gives it a chance to interact with other dislocations to form more junctions. The added stability also gives more time for the glissile arms to cross-slip and form dislocation sources. Thus, for a thicker film, dislocation multiplication could be possible due to a larger number of existing dislocations.

## **5. Concluding Remarks**

The dislocation junction and the jog in a thin film have been studied by using a modified version of ParaDiS. In a free-standing thin film, a dislocation junction with mobile arms at each end, which could act as a dislocation source through cross-slip of the arms or by interactions with other dislocations, is not easily retained. Even with the cross-slip process, the dislocation source exists only for a finite time period except for the special case in which is the two arms cross-slip simultaneously. A jogged dislocation could act as a dislocation source when it is sufficiently tall or under the high enough applied stress. However, when the jog is mobile, the source operation occurs only for the finite period of time, and the source is eventually annihilated at the free surface. Therefore, the thickness of the film limits the lifetime of both the junction and the jogged dislocation. In summary, these simulations show that dislocation multiplication seems difficult in a free-standing thin film.

## **Acknowledgements**

The work is partly supported by an NSF Career grant CMS-0547681 and an AFOSR/YIP grant. S. Aubry is supported by the Army High Performance Computing Research Center at Stanford. The support of S.-W. Lee and W. D. Nix by the Division of Materials Sciences of the Office of Basic Energy Sciences of the US Department of Energy under grant DE-FG02-04ER46163 is appreciated and gratefully acknowledged.

## References

- [1] Nix W D 1989 Mechanical properties of thin films *Met. Trans. A* **20A** 2217-2245
- [2] Nix W D, Greer J R, Feng G, Lilleodden E 2007 Deformation at the nanometer and micrometer length scales: Effects of strain gradients and dislocation starvation *Thin Solid Films* **515** 3152-3157
- [3] Hirth J P and Lothe J 1982 *Theory of Dislocations* (Malabar, FL: Krieger)
- [4] Devincere B, Kubin L P 1997 Mesoscopic simulations of dislocations and plasticity *Mater. Sci. Eng. A* **234-236** 8-14
- [5] Schwarz K W 1999 Simulation of dislocations on the mesoscopic scale. I. Methods and examples *J. Appl. Phys.* **85** 108-119
- [6] Arsenlis A, Cai W, Tang M, Rhee M, Opperstrup T, Hommes G, Pierce T G and Bulatov V V 2007 Enabling strain hardening simulations with dislocation dynamics *Modelling Simul. Mater. Sci. Eng.* **15** 553-595
- [7] Madec R, Devincere B, Kubin L P, Hoc T, Rodney D 2003 The role of collinear interaction in dislocation-induced hardening *Science* **301**1879-1882
- [8] Bulatov V V, Hsiung L L, Tang M, Arsenlis A, Bartelt M C, Cai W, Florando J N, Hiratani M, Rhee M, Hommes G, Pierce T G, Rubia T D 2006 Dislocation multi-junctions and strain hardening *Nature* **440** 1174-1178
- [9] Weinberger C R, Aubry S, Lee S.-W. Nix W D, Cai W 2009 Modelling dislocations in a free-standing thin film *Modelling Simul. Mater. Sci. Eng.* **17** 075007

- [10] Weygand D, Friedman L H, Van der Giessen E, Needleman A 2002 Aspects of boundary-value problem solutions with three-dimensional dislocation dynamics *Model. Simul. Mater. Sci. Eng.* **10** 437-468
- [11] Hartmaier A, Fivel M C, Canova G R, Gumbsch P 1999 Image stresses in a free-standing thin film *Modelling Simul. Mater. Sci. Eng.* **7** 781-793.
- [12] Tang M, Cai W, Xu G and Bulatov V V 2006 A hybrid method for computing forces on curved dislocations intersecting free surfaces in three-dimensional dislocation dynamics *Modelling Simul. Mater. Sci. Eng.* **14** 1139-1151
- [13] Nicola L, Van der Giessen E, Needleman A 2001 2D dislocation dynamics in thin metal layers *Mater. Sci. Eng. A.* **309** 274-277
- [14] Groh S, Devincre B, Kubin L P, Roos A, Feyel F, Chaboche J L 2003 Dislocations and elastic anisotropy in heteroepitaxial metallic thin films *Philos. Mag. Lett.* **83** 303-313
- [15] Wang Z, McCabe R J, Ghoniem N M, LeSar R, Misra A, Mitchell T E 2004 Dislocation motion in thin Cu foils: a comparison between computer simulations and experiment *Acta Mater.* **52** 1535-1542
- [16] Schwarz K W, Tersoff J 1996 Interaction of threading and misfit dislocations in a strained epitaxial layer *J. Appl. Phys. Lett.* **69** 1220-1222
- [17] von Blanckenhagen B, Gumbsch P, Arzt E 2003 Dislocation sources and the flow stress of polycrystalline thin metal films *Philos. Mag. Lett.* **83** 1-8
- [18] Cai W, Arsenlis A, Weinberger C R, Bulatov V V 2006 A non-singular continuum theory of dislocations *J. Mech. Phys. Solids* **54** 561-587



- [19] Madec R, Devincere B, Kubin L P 2002 From dislocation junctions to forest hardening *Phys. Rev. Lett.* **89** 255508
- [20] Motz C, Weygand D, Senger J, Gumbsch P 2009 Initial dislocation structures in 3-D discrete dislocation dynamics and their influence on microscale plasticity *Acta Mater.* **57** 1744-1754
- [21] Lee S W, Nix W D 2010 Geometrical analysis of 3D dislocation dynamics simulations of FCC micro-pillar plasticity *Mater. Sci. Eng. A* **527** 1903-1910
- [22] Weinberger C R, Cai W 2010 submitted to *Scripta Mater.*
- [23] Gruber P A, Solenthaler C, Arzt E, Spolenak R 2008 Strong single-crystalline Au films tested by a new synchrotron technique *Acta Mater.* **56** 1876-1889

**Figure 1.** Schematics of the initial conditions of junction simulations. (a) Dislocation (1) resides on the ABC plane and has the Burgers vector of BC ( $1/2[1\ 0\ \bar{1}]$ ) for the line sense vector  $\vec{\xi}_1$ . Dislocation (2) resides on the ACD plane and has the Burgers vector CD ( $1/2[1\ 0\ 1]$ ) for the line sense vector  $\vec{\xi}_2$ . This configuration produces the dislocation junction along  $[1\ \bar{1}\ 0]$  direction, which is parallel to the free surfaces. (b) Dislocation (1) resides on the ABC plane and has the Burgers vector of BD ( $1/2[0\ \bar{1}\ \bar{1}]$ ) for  $\vec{\xi}_1$ . Dislocation (2) resides on the BCD plane and has the Burgers vector CA ( $1/2[\bar{1}\ 1\ 0]$ ). This configuration produces the dislocation junction along  $[\bar{1}\ 0\ 1]$  direction, which is inclined relative to the free surface. The red arrows indicate the direction of Burgers vector for a given line sense vector,  $\xi$ .  $\alpha$  and  $\beta$  are the angles between the dislocation and the intersection and are chosen as  $\pi/9$ . Each end of both dislocations is terminated at the free surfaces. In order to see the junction formation, the two dislocations are met at the origin initially. (c) The cross-slip configuration of dislocation junction that is parallel to the free surface. The blue line CE is the junction. The dislocation arms are cross-slipped from the ACD to the CDI or equivalently, to the EFG plane. The simulations were done for the cross-slip (1) only and for both cross-slip (1) and (2) under 200 MPa along  $[100]$  direction.

**Figure 2.** Schematics of the initial condition of jogged dislocation simulations. The jog is glissile since it resides on the  $(1\ \bar{1}\ 1)$  plane. The initial structures consist of the different jog height and the same length of the dislocation arms for a given thickness. The simulations are performed under different tensile stresses along the  $[100]$  direction.

**Figure 3.** (a) The initial configuration for the dislocation junction parallel to the free surface. (b) The formation of the dislocation junction on the intersection along  $[\bar{1}\ 1\ 0]$  direction. (c) The

shrinkage of the junction. (d) The dissociation of the junction into the two separated dislocations which are repulsive to each other. The inset shows the dislocations in (d) from a different viewpoint.

**Figure 4.** (a) The initial configuration of two dislocations. (b) and (c) are the intermediate and final stage of LC junction formation, respectively. The dislocation junction forms along  $[ \bar{1} 0 1 ]$  direction. After the relaxation, only the immobile junction remains in the thin film.

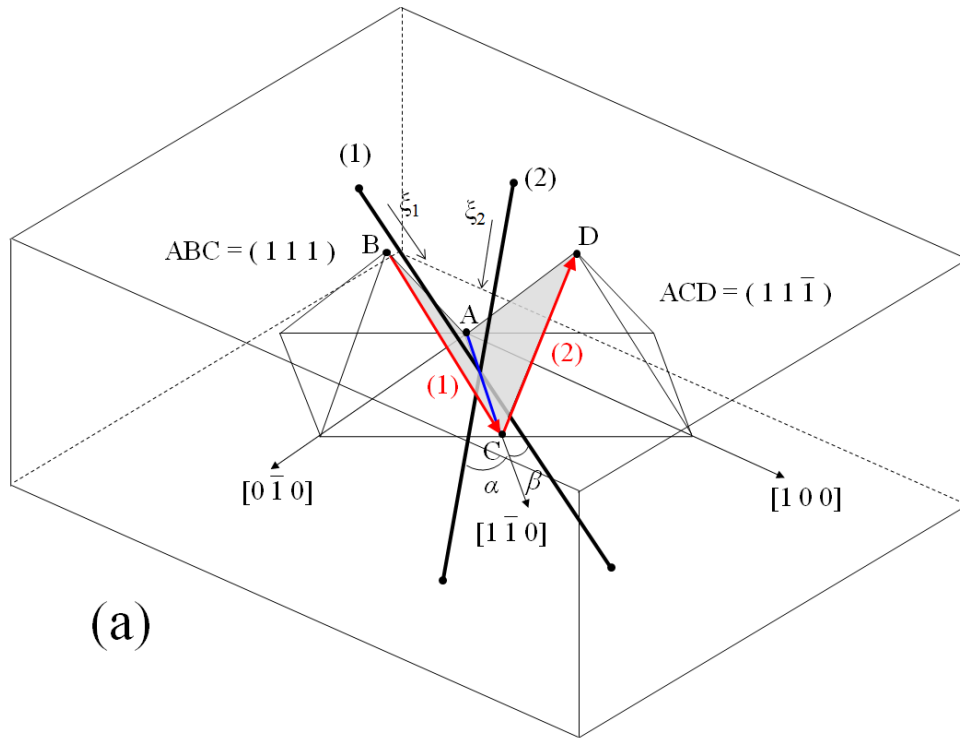
**Figure 5.** The unzipping process and source operation of a dislocation junction parallel to the free surface. Here, the one dislocation arm on dislocation (2) is cross-slipped initially.

**Figure 6.** The formation and annihilation of the dislocation dipole under 100 MPa in a 1  $\mu\text{m}$  thick film. Here the jog height is  $25b$ . The insets in (a) show the magnified view of the jog. The dipole is eventually annihilated at the free surface. The dashed line shows the direction along which the jog can glide. The red arrow shows the direction of dipole motion.

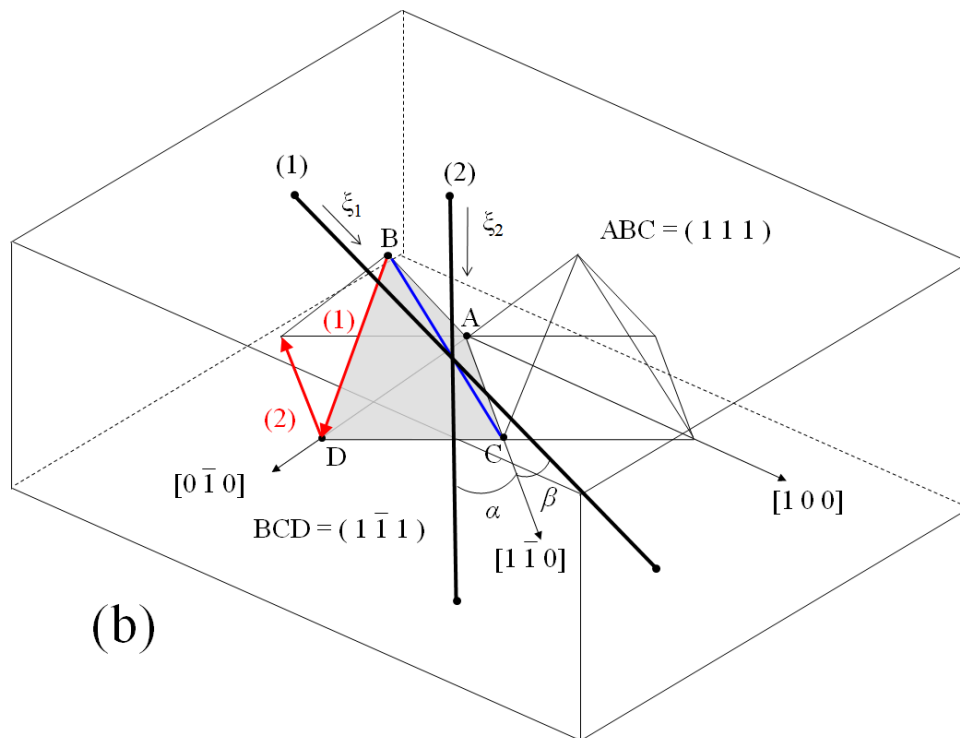
**Figure 7.** The operation of double arm source under 200 MPa in a 1  $\mu\text{m}$  thick film. Here the jog height is  $25b$ . The dashed line shows the direction along which the jog can glide. The red arrow indicates the location of the slip plane intersection. The dynamic source is destroyed when the anchoring point is annihilated at the free surface in figure 9(c).

**Figure 8.** The mechanism map for 1  $\mu\text{m}$  thick film. The dotted lines are the boundary between the different mechanisms, and they are obtained from equation (1) (B1) and (2) (B2).

Figure 1



(a)



(b)

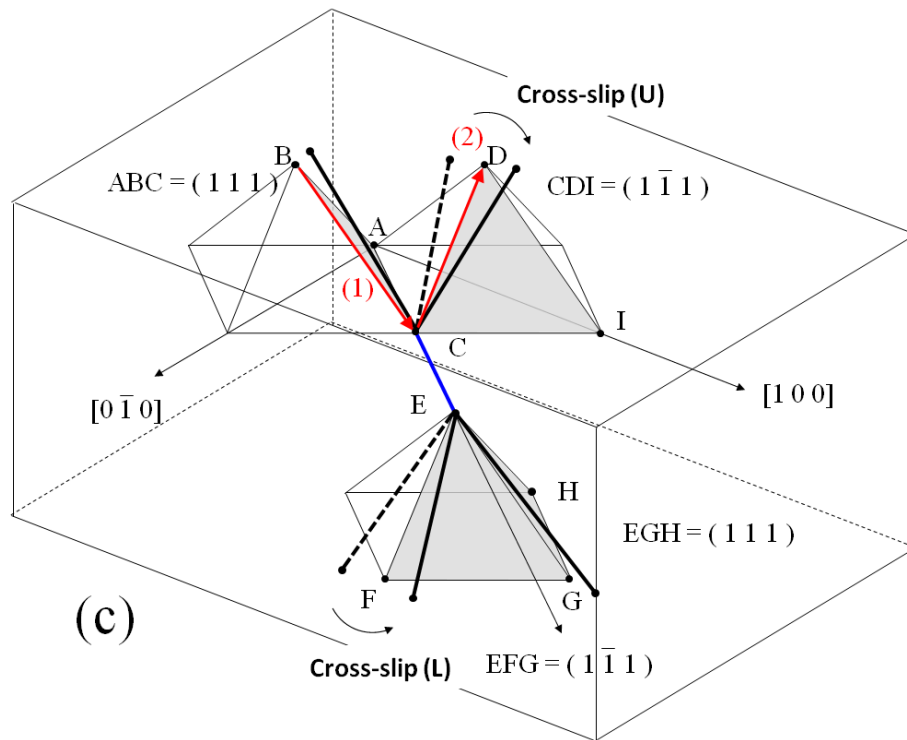


Figure 2.

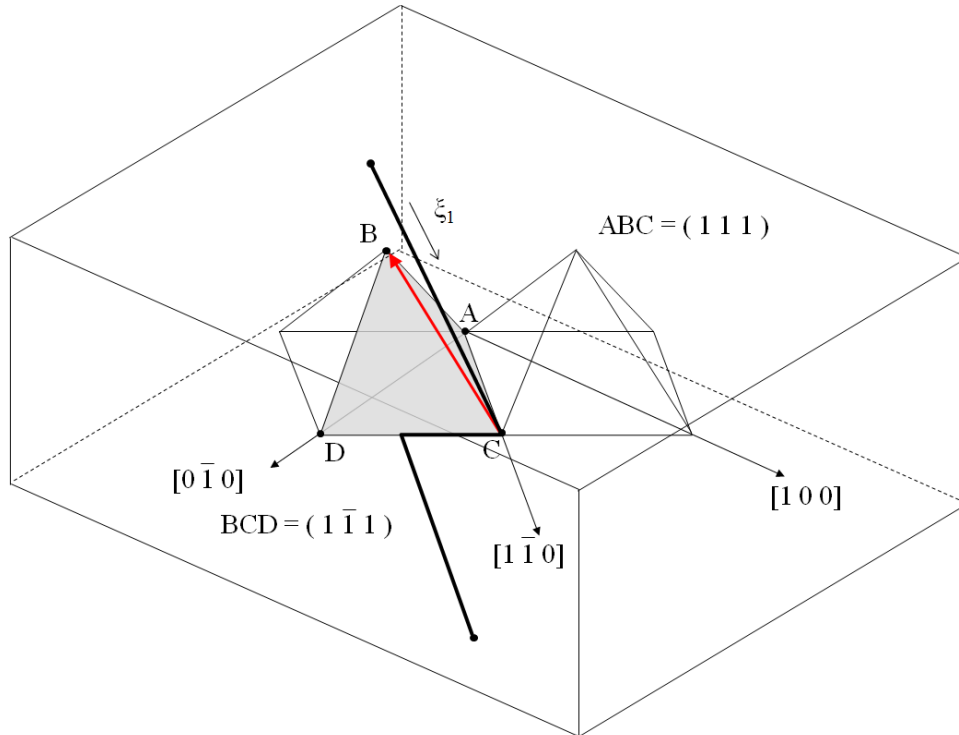


Figure 3.

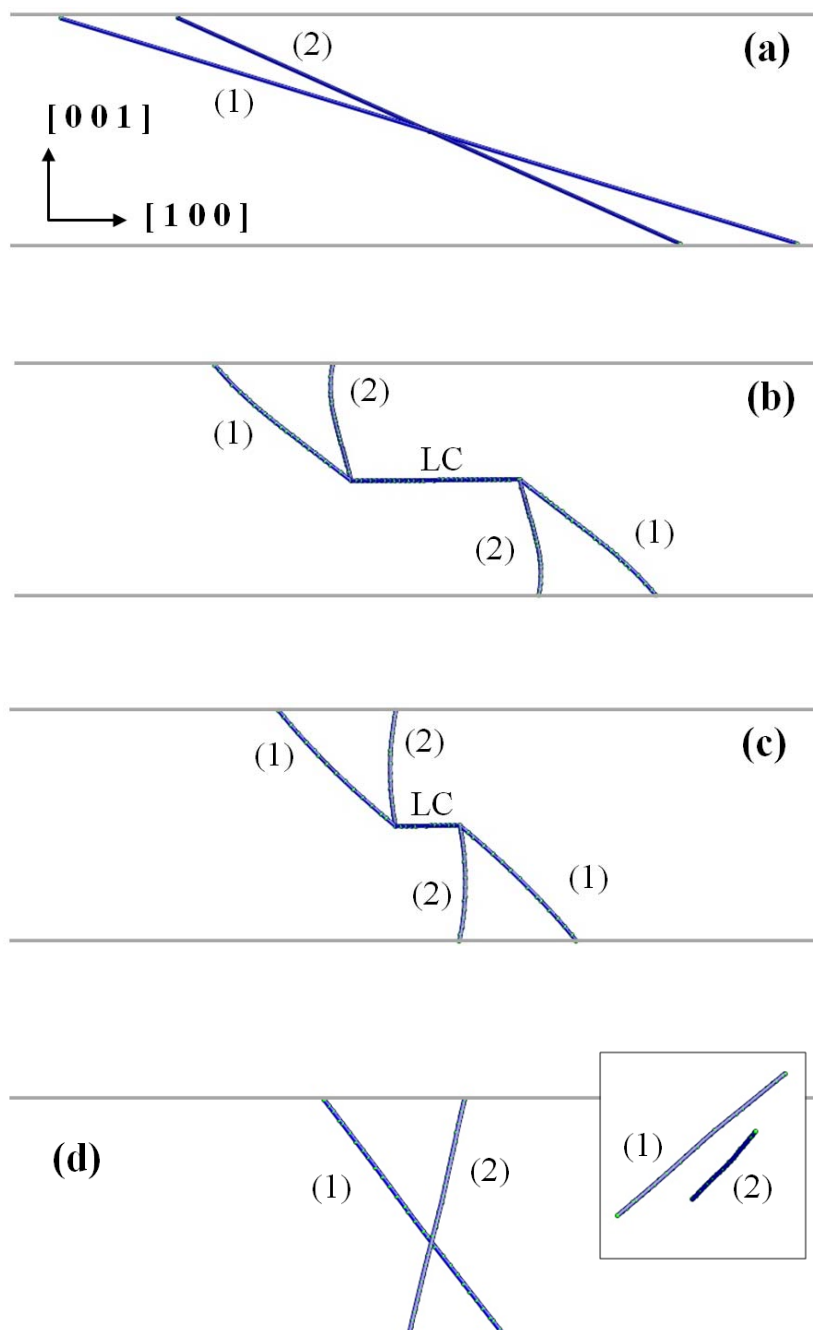


Figure 4.

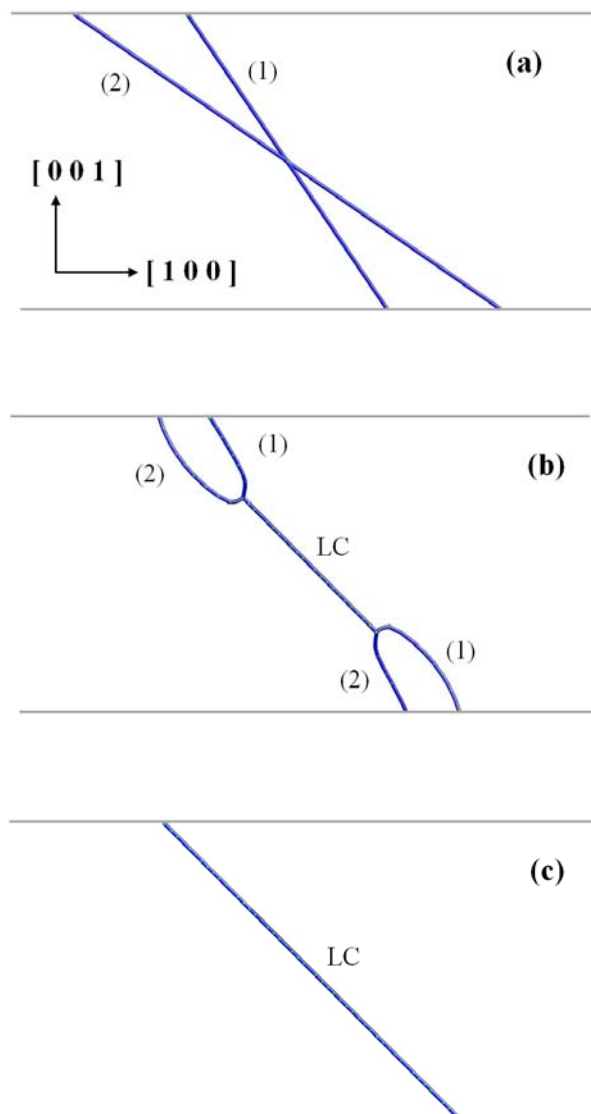




Figure 5.

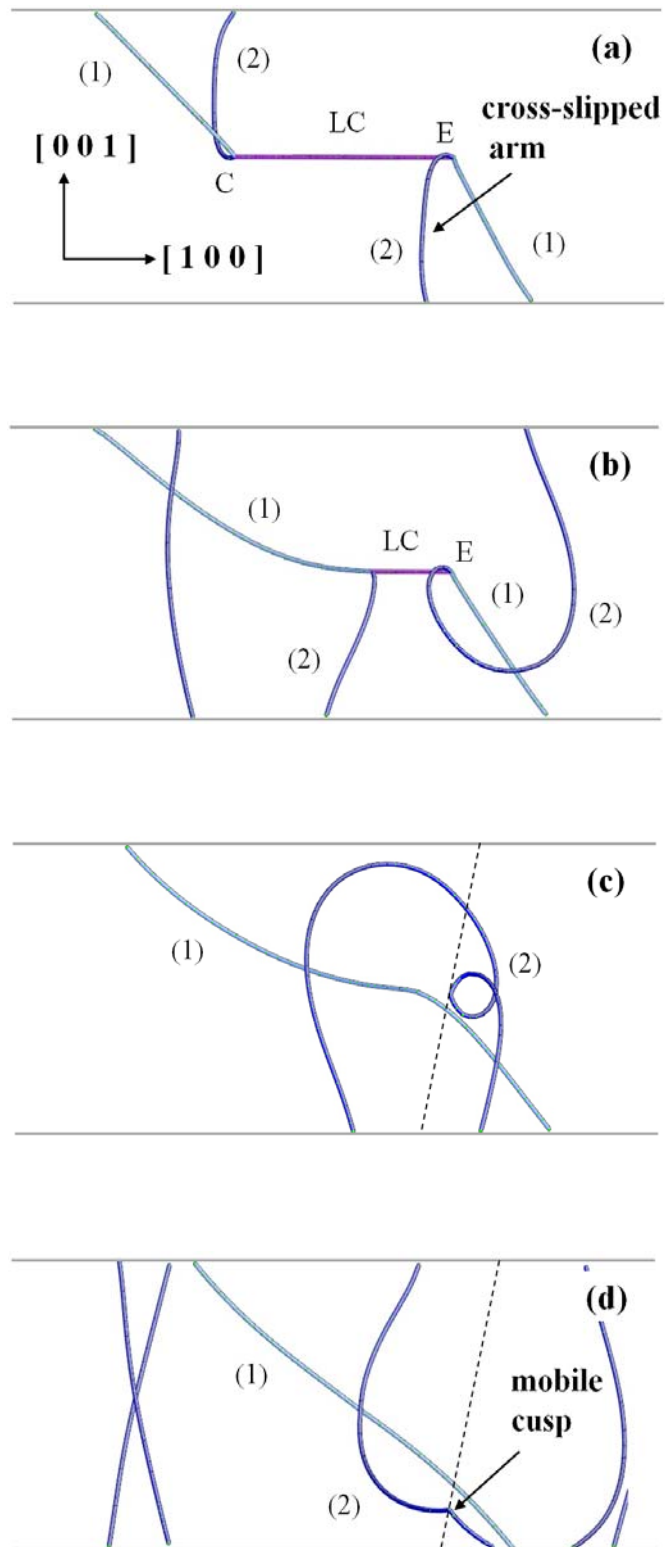


Figure 6.

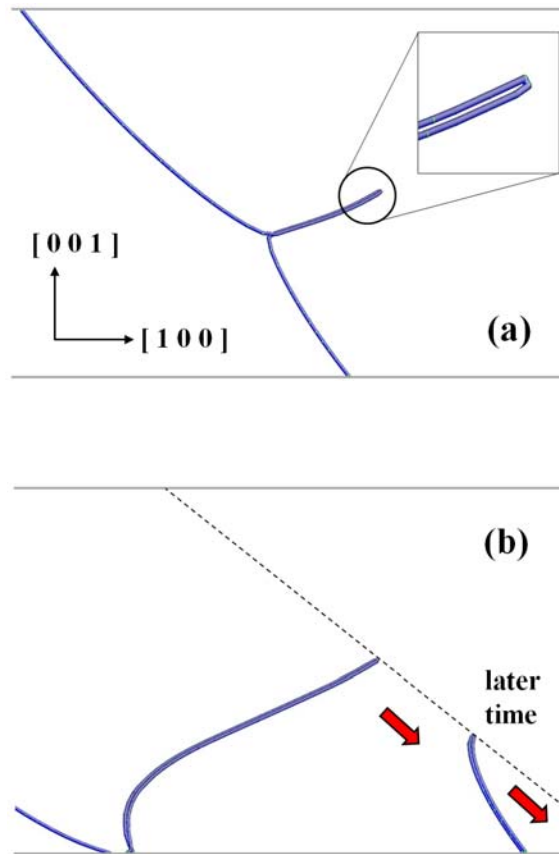


Figure 7.

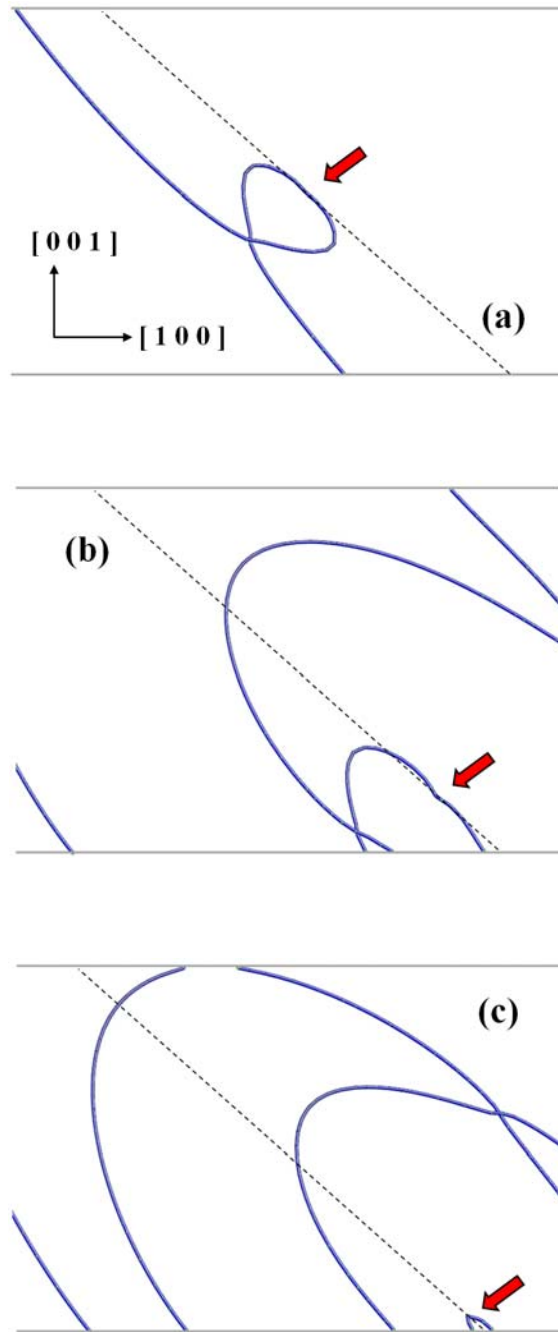


Figure 8.

